

Asking for an extra photon in Higgs production at the LHC and beyond

Emidio Gabrielli,^a Barbara Mele,^b Fulvio Piccinini^c and Roberto Pittau^d

^a*Dipart. di Fisica Teorica, Università di Trieste, Strada Costiera 11, I-34151 Trieste, Italy, INFN, Sezione di Trieste, Via Valerio 2, I-34127 Trieste, Italy, and NICPB, Ravala 10, Tallinn 10143, Estonia*

^b*INFN, Sezione di Roma, c/o Dipart. di Fisica, "Sapienza" Università di Roma, P.le Aldo Moro 2, I-00185 Rome, Italy*

^c*INFN, Sezione di Pavia, Via A. Bassi 6, I-27100 Pavia, Italy*

^d*Departamento de Física Teórica y del Cosmos and CAFPE, Universidad de Granada, Campus Fuentenueva s.n., E-18071 Granada, Spain*

E-mail: emidio.gabrielli@cern.ch, barbara.mele@roma1.infn.it, fulvio.piccinini@pv.infn.it, pittau@ugr.es

ABSTRACT: We study the inclusive production of a Higgs boson in association with a high- p_T photon at the LHC, detailing the leading-order features of the main processes contributing to the $H\gamma$ final state. Requiring an extra hard photon in Higgs production upsets the cross-section hierarchy for the dominant channels. The $H\gamma$ inclusive production comes mainly from photons radiated in vector-boson fusion (VBF), which accounts for about 2/3 of the total rate, for $p_T^{\gamma,j} > 30$ GeV, at leading order. On the other hand, radiating a high- p_T photon in the main top-loop Higgs channel implies an extra parton in the final state, which suppresses the production rate by a further α_S power. As a result, the $H\gamma$ production via top loops at the LHC has rates comparable with the ones arising from either the $Ht\bar{t}$ production or the $HW(Z)\gamma$ associated production. Then, in order of decreasing cross section, comes the single-top-plus-Higgs channel, followed in turn by the heavy-flavor fusion processes $b\bar{b} \rightarrow H\gamma$ and $c\bar{c} \rightarrow H\gamma$. The $H\gamma$ production via electroweak loops has just a minor role. At larger c.m. energies, the $Ht\bar{t}\gamma$ channel surpasses the total contribution of top-loop processes. In particular, requiring $p_T^{\gamma,j} > 30$ GeV at $\sqrt{S} \simeq 100$ TeV, $Ht\bar{t}\gamma$ accounts for about 1/4 of the inclusive $H\gamma$ production at leading order, about half of the total being due to VBF production.

Contents

1	Introduction	1
2	Processes contributing to the $H\gamma$ final state	3
2.1	QCD production via top loops in $gg, qg(\bar{q}g), \bar{q}q \rightarrow H\gamma j$	4
2.2	Vector boson fusion	7
2.3	Associated HW and HZ production	8
2.4	Top-pair and single-top final states	8
2.5	Heavy-quark $b\bar{b}, c\bar{c}$ fusion	10
2.6	Electroweak $\bar{q}q \rightarrow H\gamma$ production	11
3	Comparison of rates and distributions	11
4	Conclusions	15
A	Asymptotic behavior of the top pentagon amplitude for $gg \rightarrow H\gamma g$.	17

1 Introduction

The observation of a Higgs boson signal at the LHC [1] opened up a new era for collider physics. On the one hand, a major task of the LHC and future high-energy colliders is now to verify with high accuracy the actual properties of the new state, in order to check whether the standard model (SM) really provides the complete description of the electroweak symmetry breaking (EWSB) through the Higgs mechanism [2] at the TeV energy scale, or some theory modification is needed. On the other hand, Higgs boson production in the SM can itself act as a background for new possible exotic states that might involve Higgs bosons in their production or decay channels. As a consequence, the most accurate predictions on both Higgs production mechanisms and Higgs decay characteristics in the SM are desirable.

In this paper, we discuss the Higgs production associated to a prompt high- p_T photon at the LHC. The $H\gamma$ final state can be experimentally quite distinctive, and might probe $H\gamma$ interactions in a nontrivial way. After requiring an extra high- p_T photon, the naive expectation is that the original Higgs production mechanisms should be suppressed by a few order of magnitudes, corresponding to an extra α factor in cross sections (where $\alpha = e^2/4\pi$), while maintaining their relative weight. Actually, the main Higgs production mechanisms react in different ways to the requirement of photon radiation. In particular, we will show here that the normal hierarchy in the Higgs production channels is upset by the requirement of an extra high p_T photon.

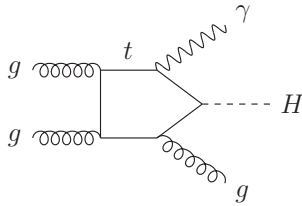


Figure 1. Basic top-quark pentagon diagram contributing to $gg \rightarrow H\gamma g$.

Higgs production at the LHC mainly proceeds, in order of decreasing rate, via gluon-gluon (gg) fusion (mostly through a top-quark loop), vector-boson fusion (VBF), associated VH production (where V is either a W or a Z boson), associated $t\bar{t}H$ and $b\bar{b}H$ production, and single-top tH production. Predictions for the corresponding cross sections have been worked out with good accuracy (including at least QCD NLO corrections for all processes [3]). At the LHC, there is then a substantial hierarchy in the corresponding cross sections, and the gluon-fusion production via a top-loop turns out to be by far the dominant contribution to the inclusive Higgs production, being an order of magnitude higher than the VBF process, as detailed in the following.

The request of an extra photon in the final state changes drastically the latter ordering. Indeed, the process $gg \rightarrow H\gamma$, occurring via a top-box diagram, is forbidden by Furry's theorem, and in general by C parity. Then, the lowest-order partonic processes proceeding via QCD interactions (and unsuppressed by small Yukawa couplings) are either the light-quark initiated processes $gq(\bar{q}) \rightarrow H\gamma q(\bar{q})$ and $q\bar{q} \rightarrow H\gamma g$ (both involving a top-loop ggH vertex) or $gg \rightarrow H\gamma g$ (via a pentagon top loop) [Figure 1]. The contribution of the $gg \rightarrow H\gamma g$ amplitude to the $H\gamma j$ rate has been recently evaluated in [4], where the latter process is claimed to be responsible for the dominant production of $H\gamma j$ final states at the LHC, followed by the heavy-quark $Q\bar{Q}, gQ$ scattering into $H\gamma$.

In the present study, we will show that the $gg \rightarrow H\gamma g$ channel actually contributes to the inclusive $H\gamma j$ production to a much lesser extent than previously stated. Indeed, on the one hand, the ggH -loop-mediated production via the t -channels $gq(\bar{q}) \rightarrow H\gamma q(\bar{q})$ will be found to be about one order of magnitude larger than the one mediated by the top-pentagon amplitude $gg \rightarrow H\gamma g$ at the LHC. On the other hand, the actual (by far) dominant production of $H\gamma$ final states accompanied by jets will turn out to proceed through an electroweak process, that is the VBF Higgs production $q\bar{q} \rightarrow H\gamma q\bar{q}$, where the high- p_T photon radiation by the initial/final quarks, connected by W charged currents, is enhanced by the absence of suppressive QCD coherence effects [5, 6].

We will also evaluate for the first time the contributions to the inclusive $H\gamma$ production arising from a hard photon radiated in the associated production of a Higgs plus either a top-quark pair in $Ht\bar{t}$ final states or a single top in the t -channel Ht ($H\bar{t}$) production. The $Ht\bar{t}\gamma$ will be found to contribute at the LHC at the same level as the $gq(\bar{q}) \rightarrow H\gamma q(\bar{q})$ channels. Remarkably, the relative $Ht\bar{t}\gamma$ weight increases at larger c.m. energies, approaching the relative (still dominant) contribution of the VBF component at $\sqrt{S} \sim 100$ TeV. The $Ht\gamma$ component is of course lower than the $Ht\bar{t}\gamma$ one, but less than naively expected, thanks

to the enhancing mechanism related to the W -exchange in the t -channel Ht production, similar to the one acting in the VBF case [5, 6].

The $HV\gamma$ (with $V = W, Z$) associated production has been evaluated in [7, 8] at the NLO in QCD. As we will see, at the LHC energies, it also contributes to the $H\gamma$ production in a comparable way to the t -channels $gq(\bar{q}) \rightarrow H\gamma q(\bar{q})$ (and to the $Ht\bar{t}\gamma$ process).

We then reconsider the total contribution to the $H\gamma$ final states of the heavy-flavour ($b\bar{b}$ and $c\bar{c}$) scattering [9], that will be found comparable to the $gg \rightarrow H\gamma g$ process at the LHC. We finally comment on the minor $H\gamma$ component due the $q\bar{q} \rightarrow H\gamma$ electroweak-loop process previously studied in [9].

We stress that the present study is not aimed to provide the most accurate estimate of the production cross sections for different $H\gamma$ channels, but rather to analyze the inclusive production of the $H\gamma$ system through its main components, discussing the corresponding relative weight. Such a discussion has non-trivial aspects that, to our knowledge, have not previously been detailed in the literature.

The plan of the paper is the following. In Section 2, we discuss the cross-section computation for the different channels contributing to the $H\gamma$ final state in proton-proton collisions. For some processes, a QCD next-to-leading-order (NLO) evaluation is available, for others, even the tree-level estimates are, to our knowledge, still missing in the literature, and we provide them here. In particular, we present LO $H\gamma$ cross sections relevant for LHC and future higher-energy pp colliders. In Section 3, we compare the different contributions, looking at both total rates and Higgs/photon kinematical distributions. Hierarchies of $H\gamma$ cross sections are then compared with the ordering of original Higgs production mechanisms. In Section 4, we present our conclusions and outlook. In the Appendix, we report the asymptotic behavior of the top pentagon amplitude for the $gg \rightarrow H\gamma g$ channel.

2 Processes contributing to the $H\gamma$ final state

In this section, we detail the present theoretical knowledge of the various channels contributing to the associated production of a Higgs boson and a high- p_T photon at the LHC. For a few of them QCD NLO predictions are available, others have been computed only at leading order (LO), while some processes like the Higgs production in association with top quarks to our knowledge have not yet been considered in the literature. We will discuss the main processes in order of decreasing relevance of the corresponding channels with no photon emission, which are responsible for the dominant Higgs boson production at the LHC. Remarkably, we will see that the request of an extra high- p_T photon in the basic Higgs production processes will have a strong impact on the relative weight of different channels.

When quoting the $H\gamma$ production rates in the present study, we will assume common sets of input parameters and kinematical cuts. The latter are needed in most of the channels considered, which are characterized by collinear- and soft-photon (and -parton) divergencies.

The setup applied in all cross-section computations (even in absence of divergencies) is

$$\begin{aligned} p_T^\gamma &> 30 \text{ GeV}, & |\eta_\gamma| &< 2.5, \\ p_T^j &> 30 \text{ GeV}, & |\eta_j| &< 5, \\ \Delta R(\gamma, j_i) &> 0.4, & \Delta R(j_1, j_2) &> 0.4, \end{aligned} \tag{2.1}$$

where $\Delta R(a, b) = \sqrt{\Delta\phi(a, b)^2 + \Delta\eta(a, b)^2}$ is the angular separation between a and b , and j_i ($i = 1, 2$) is any parton in the final state. We then set the Higgs and the heavy quark masses as follows :

$$\begin{aligned} m_H &= 125 \text{ GeV}, & m_t &= 173 \text{ GeV}, \\ m_b^{\overline{MS}}(m_H) &= 2.765 \text{ GeV}, & m_c^{\overline{MS}}(m_H) &= 0.616 \text{ GeV}, \end{aligned} \tag{2.2}$$

where we assumed the running masses at the m_H scale in the Yukawa couplings entering the $b\bar{b}, c\bar{c} \rightarrow H\gamma$ cross sections.

In the present analysis, we are mainly interested in establishing the relative importance of the main processes giving rise to $H\gamma$ final states. Since, for most of the channels we will analyze in the following, QCD NLO cross sections have not yet been computed, in order to make a consistent comparison, we will always consider QCD LO rates (even when QCD NLO estimates are already available in the literature).

When considering the absolute rates that we will present below, one should then keep in mind the influence of the cut choice on the cross sections. In Section 3, we will show how relaxed requirements on kinematics can influence the relative weight of different channels.

To compute LO cross sections and distributions we use `AlpGen` [10]¹, with the parton distribution set CTEQ5L [11], setting the factorization (μ_F) and renormalization (μ_R) scale at the common value $\mu = m_H$. We will estimate the LO cross-section uncertainties by varying $\mu = \mu_F = \mu_R$ in the range $[\frac{1}{2} m_H, 2 m_H]$.

In the next subsections, we will report cross sections for the different channels according to the parameters and settings described above, for proton collision c.m. energies of 14 TeV, 33 TeV and 100 TeV, the latter being relevant for Future Circular Collider (FCC) studies that are presently under way [12]². Proton collisions at 33 TeV could be realized in an upgraded-energy program of the LHC (usually named HE-LHC [15]).

2.1 QCD production via top loops in $gg, qg(\bar{q}g), \bar{q}q \rightarrow H\gamma j$

When asking for an extra photon in the main Higgs production channel $gg \rightarrow H$ proceeding via gluon fusion into a top triangle loop, one is forced to pass to the next QCD order, and include an extra parton in the collision final state. Indeed, as already mentioned, Furry's theorem forbids the emission of a photon from the ggH top-quark loop, and the

¹Since not all processes treated in this study are available in the official release `v2.14`, we have extended the code, to include also the processes $gg, q\bar{q} \rightarrow H\gamma t\bar{t}$, $b\bar{q} \rightarrow H\gamma t\bar{q}$, $Q\bar{Q} \rightarrow H\gamma$ and $Q\bar{Q} \rightarrow H$ with $Q = b, c$.

²Physics and, in particular, Higgs physics at 100 TeV have been recently reviewed in [13] and [14], respectively.

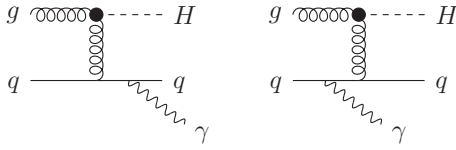


Figure 2. Feynman diagrams for $gq \rightarrow H\gamma q$. The black blob represents the ggH effective vertex.

$gg \rightarrow H\gamma$ amplitude vanishes³. Then, one can either require a further gluon emission in the latter process, and obtain a non-vanishing $gg \rightarrow H\gamma g$ amplitude via a top pentagon loop (Figure 1), or ask for an extra photon radiation in the Higgs+jet production proceeding via the channels $gq \rightarrow Hq$ ($g\bar{q} \rightarrow H\bar{q}$), and $\bar{q}q \rightarrow Hg$ by means of a top triangle loop (Figure 2 and 3, respectively).

The production of $H\gamma j$ final states from the gluon fusion $gg \rightarrow H\gamma g$ channel at hadron colliders has been recently studied in [4]. The $gg \rightarrow H\gamma g$ amplitude is gauge invariant and finite, and one can compute the gluon-fusion separate contribution to $H\gamma$ production. In our analysis, we have redone the evaluation of the top pentagon amplitude $\mathcal{A}_{\text{Pent}}$ associated to the $gg \rightarrow H\gamma g$ channel. We detail our computation in the following.

$\mathcal{A}_{\text{Pent}}$ is given by the sum of the 24 pentagon-like diagrams obtained by permuting in all possible ways the external vectors in Figure 1. Each diagram can be expressed in terms of a linear combination of one-loop scalar boxes, triangles, bubbles, massive tadpoles and rational terms. The coefficients of all scalar functions have been obtained numerically via the OPP approach [16], as implemented in `CutTools` [17], linked to the one-loop scalar functions in [18]. As each pentagon is separately ultraviolet (UV) convergent, no rational term of the R_2 kind is present [19]. Thus, the full rational part of $\mathcal{A}_{\text{Pent}}$ is R_1 -like, and also numerically provided by `CutTools`.

The input needed by `CutTools` is the integrand of each diagram as a function of the integration momentum. In order to speed up the computation, we have used an in-house implementation of the massive helicity method [20] that expresses traces over gamma matrices in terms of scalar products in the spinor space. This gives a numerical stable answer for most of the phase-space points. In order to detect and rescue the remaining unstable configurations, we have used the built-in quadruple-precision facilities of `CutTools`. As a result, no randomly generated phase-space point is discarded during the Monte Carlo integration. As for the latter, the value of $|\mathcal{A}_{\text{Pent}}|^2$ computed by `CutTools` is plugged into a code based on `AlpGen`, which, besides integrating over the relevant phase-space, also takes care of the convolution with the gluon parton densities⁴.

In order to validate the correctness of our calculation, a numerical check of gauge invariance has been performed. In particular, we have numerically replaced polarization vectors by four-momenta, obtaining zero up to the machine precision. In addition, we have

³Note that the vanishing of the $gg \rightarrow H\gamma$ amplitude is a general consequence of C parity, which holds in any SM theory extension.

⁴The corresponding numerical code is available in <http://www.ugr.es/~pittau/PENTAGON/>.

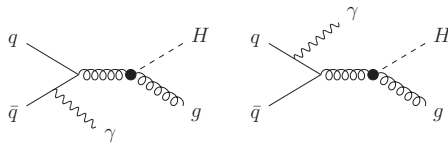


Figure 3. Feynman diagrams for $q\bar{q} \rightarrow H\gamma g$. The black blob represents the ggH effective vertex.

checked the numerical agreement between the result obtained when using a large input value for the top mass and the analytic asymptotic behavior of $\mathcal{A}_{\text{Pent}}$, as reported in the Appendix.

Finally, we have compared our outcome for the $gg \rightarrow H\gamma g$ channel with the results in [4], and found complete agreement on both numerical cross sections and kinematical distributions. We stress that there is no infrared divergence for either photons or gluons in the final state, and the maximum of the corresponding p_T distributions is ruled by the top mass circulating in the pentagon loop. In particular, the photon and gluon p_T distributions are both peaked at $p_T^{\text{max}} \sim 120$ GeV at 14 TeV, while the Higgs distribution is maximal at $p_T^{\text{max}} \sim 80$ GeV [4].

The $gg \rightarrow H\gamma g$ cross section corresponding to the setup in Eqs. (2.1)-(2.2) is

$$\sigma(gg \rightarrow H\gamma g)^{\sqrt{S}=14 \text{ TeV}} = 0.287^{+0.138}_{-0.086} \text{ fb}, \quad (2.3)$$

$$\sigma(gg \rightarrow H\gamma g)^{\sqrt{S}=33 \text{ TeV}} = 1.79^{+0.71}_{-0.47} \text{ fb}, \quad (2.4)$$

$$\sigma(gg \rightarrow H\gamma g)^{\sqrt{S}=100 \text{ TeV}} = 12.0^{+3.6}_{-2.6} \text{ fb}, \quad (2.5)$$

where the cross section *central value* assumes $\mu_F = \mu_R = m_H$, and the upper (lower) variations correspond to $\mu_F = \mu_R = \frac{1}{2}m_H$ ($\mu_F = \mu_R = 2m_H$).

In [4], the $gg \rightarrow H\gamma g$ rate has been compared to the heavy-quark $Q\bar{Q} + Qg \rightarrow H\gamma j$ cross section (with $Q = b, c$), and claimed to provide the dominant contribution to the $H\gamma j$ final state at hadron colliders. Here, we correct the latter statement, by including also the $H\gamma j$ production initiated by light quarks, proceeding via the top triangle ggH vertex in either the t -channel (Figure 2) or the s -channel (Figure 3). The corresponding LO cross section (summing up over the t and s channels, and assuming the same set of cuts and conventions as above) have been obtained by `AlpGen`, by a ggH effective vertex :

$$\sigma(gq, g\bar{q}, q\bar{q} \rightarrow H\gamma q, \bar{q}, g)^{\sqrt{S}=14 \text{ TeV}} = 2.77^{+0.40}_{-0.34} \text{ fb}, \quad (2.6)$$

$$\sigma(gq, g\bar{q}, q\bar{q} \rightarrow H\gamma q, \bar{q}, g)^{\sqrt{S}=33 \text{ TeV}} = 11.1^{+1.1}_{-0.9} \text{ fb}, \quad (2.7)$$

$$\sigma(gq, g\bar{q}, q\bar{q} \rightarrow H\gamma q, \bar{q}, g)^{\sqrt{S}=100 \text{ TeV}} = 54.0^{+1.9}_{-2.0} \text{ fb}. \quad (2.8)$$

Note that the s -channel $q\bar{q} \rightarrow H\gamma g$ cross section provides a tiny component to the latter rates, amounting to about 2.8% of the total cross section at 14 TeV, and 1.9% at 100 TeV.

As a result, at the 14-TeV LHC, the light-quark initiated contribution to the $H\gamma j$ production turns out to be an order of magnitude larger than the pentagon gluon-fusion

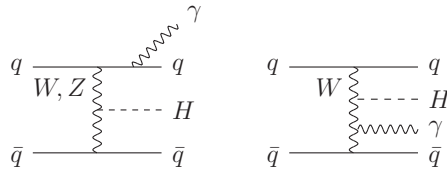


Figure 4. Two representative diagrams for the VBF channel $q\bar{q} \rightarrow H\gamma q\bar{q}$.

production (*cf.* Eqs. (2.3) and (2.6)).

2.2 Vector boson fusion

The Higgs-photon associated production in VBF is obtained by the emission of a high- p_T photon from either the initial/final quarks or the t -channel W propagators, as shown in Figure 4 for two representative diagrams out of the complete set. The $q\bar{q} \rightarrow H\gamma q\bar{q}$ channel⁵ has been studied at LO in [5], and at NLO in [6]. Apart from the setup detailed in Eqs. (2.1)-(2.2), we will assume a further cut on the quark-pair invariant mass, $M_{j_1, j_2} > 100$ GeV, hence depleting the contribution from the $q\bar{q} \rightarrow HW/HZ$ associated production, which will be considered separately in the following.

Asking for an extra high- p_T photon in VBF drastically increases the relative importance of the WW fusion component with respect to the ZZ one [5]. Indeed, in the ZZ fusion channel, destructive-interference effects occur between the photon radiation from initial and final quarks connected by a t -channel Z exchange. As a result, while asking for an extra central photon with $p_T \gtrsim 20$ GeV typically suppresses the WW -fusion cross section by two orders of magnitude, the corresponding decrease in the ZZ component is $\mathcal{O}(10^{-3})$. This makes the ZZ fusion contribution to the total $q\bar{q} \rightarrow H\gamma q\bar{q}$ cross section even smaller than naively expected, and almost negligible [5].

The total LO cross section for $q\bar{q} \rightarrow H\gamma q\bar{q}$, computed by **AlpGen**, is

$$\sigma(q\bar{q} \rightarrow H\gamma q\bar{q})^{\sqrt{S}=14 \text{ TeV}} = 22.0^{+1.3}_{-1.1} \text{ fb}, \quad (2.9)$$

$$\sigma(q\bar{q} \rightarrow H\gamma q\bar{q})^{\sqrt{S}=33 \text{ TeV}} = 87.3^{+0.3}_{-0.0} \text{ fb}, \quad (2.10)$$

$$\sigma(q\bar{q} \rightarrow H\gamma q\bar{q})^{\sqrt{S}=100 \text{ TeV}} = 325. \text{ }^{+23}_{-20} \text{ fb}. \quad (2.11)$$

The VBF contribution is then found to be by far dominant over the top-loop mediated channels contributing to $H\gamma$ final states. In particular, $\sigma(q\bar{q} \rightarrow H\gamma q\bar{q})$ is almost an order of magnitude larger than $\sigma(gq, g\bar{q}, q\bar{q} \rightarrow H\gamma q, \bar{q}, g)$ at the LHC (*cf.* Eq. (2.6)), and six times higher at 100 TeV (*cf.* Eq. (2.8)). Note that here we are applying a $p_T > 30$ GeV requirement on forward jets, that is quite stricter than the 20-GeV cut usually applied in VBF studies at the LHC, hence considerably reducing the predicted cross sections. In Section 3, we will discuss the effect of relaxing the relevant cuts on transverse momenta.

⁵The possibility of different quark flavors in initial and final states is understood in our notation.

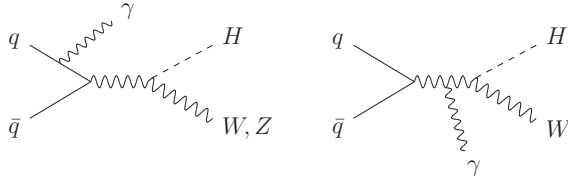


Figure 5. Two representative diagrams for the $HV\gamma$ associated production.

Contributions to the $H\gamma jj$ production different from VBF can arise from the NLO treatment of the $gg, qg(\bar{q}g), \bar{q}q \rightarrow H\gamma j$ channels analyzed in Section 2.1. These are expected to be quite depleted with respect to VBF [5], and will not be considered in this analysis.

2.3 Associated HW and HZ production

The $H\gamma$ final states arising from the associated production $q\bar{q} \rightarrow HW, q\bar{q} \rightarrow HZ$ derive from the emission of a hard photon from the $q\bar{q}$ initial state, and, in the HW case, from either the W propagator or the final W (see Figure 5 for two representative diagrams out of the complete set). NLO predictions for $q\bar{q} \rightarrow H\gamma W$ and $q\bar{q} \rightarrow H\gamma Z$ have been presented in [7] and [8], respectively (see also [21]).

Our `AlpGen` estimates for the corresponding LO cross sections are

$$\sigma(q\bar{q} \rightarrow H\gamma W)^{\sqrt{S}=14 \text{ TeV}} = 1.87_{+0.02}^{-0.03} \text{ fb}, \quad (2.12)$$

$$\sigma(q\bar{q} \rightarrow H\gamma W)^{\sqrt{S}=33 \text{ TeV}} = 5.19_{+0.32}^{-0.37} \text{ fb}, \quad (2.13)$$

$$\sigma(q\bar{q} \rightarrow H\gamma W)^{\sqrt{S}=100 \text{ TeV}} = 16.5_{+2.1}^{-2.2} \text{ fb}, \quad (2.14)$$

and

$$\sigma(q\bar{q} \rightarrow H\gamma Z)^{\sqrt{S}=14 \text{ TeV}} = 1.34_{+0.03}^{-0.03} \text{ fb}, \quad (2.15)$$

$$\sigma(q\bar{q} \rightarrow H\gamma Z)^{\sqrt{S}=33 \text{ TeV}} = 3.49_{+0.23}^{-0.28} \text{ fb}, \quad (2.16)$$

$$\sigma(q\bar{q} \rightarrow H\gamma Z)^{\sqrt{S}=100 \text{ TeV}} = 10.3_{+1.4}^{-1.4} \text{ fb}. \quad (2.17)$$

At the LHC, the sum of the latter contributions amounts roughly to the total top-loop induced cross sections in Eqs. (2.3) and (2.6).

2.4 Top-pair and single-top final states

The Higgs production via top-pair final states offers the unique opportunity to directly test the top Yukawa coupling. This channel is quite depleted with respect to the gg , VBF, and HV -associated production because of m_t phase-space effects. Requiring an extra hard photon in the $Ht\bar{t}$ final states affects this hierarchy, since high- p_T photons are more naturally radiated in the production of (more spherical) massive charged systems (see Figure 6 for two representative diagrams out of the complete set). The $H\gamma t\bar{t}$ cross section computed at

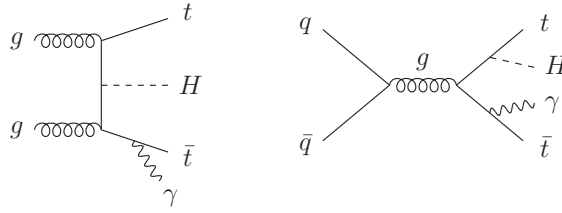


Figure 6. Two representative diagrams for $gg, q\bar{q} \rightarrow H\gamma t\bar{t}$.

LO via `AlpGen` is

$$\sigma(gg, q\bar{q} \rightarrow H\gamma t\bar{t})^{\sqrt{S}=14 \text{ TeV}} = 2.55^{+0.89}_{-0.60} \text{ fb}, \quad (2.18)$$

$$\sigma(gg, q\bar{q} \rightarrow H\gamma t\bar{t})^{\sqrt{S}=33 \text{ TeV}} = 17.8^{+5.4}_{-3.8} \text{ fb}, \quad (2.19)$$

$$\sigma(gg, q\bar{q} \rightarrow H\gamma t\bar{t})^{\sqrt{S}=100 \text{ TeV}} = 159.^{+37}_{-29} \text{ fb}. \quad (2.20)$$

The LHC $H\gamma t\bar{t}$ cross section turns out to be in the same ballpark of the top-loop $H\gamma j$ cross section, and also of the total $H\gamma V$ cross section (with $V = W, Z$). At larger \sqrt{S} , the $H\gamma t\bar{t}$ rate gets the upper hand, and approaches the VBF $H\gamma q\bar{q}$ rate. At 100 TeV, the $H\gamma t\bar{t}$ rate is just about half the VBF $H\gamma q\bar{q}$ one, and we will see that the $H\gamma t\bar{t}$ channel becomes the second most important production mechanism for $H\gamma$ final states.

The Higgs production associated to a single top is an electroweak process that can proceed via three different channels at hadron colliders [22]. Here, we restrict to the t -channel $b\bar{q} \rightarrow tH\bar{q}$ which has the largest cross section. The t -channel rate is anyway quite small at the LHC. Nevertheless, its role has recently been emphasized for its sensitivity to a possible change in the relative sign of the ttH and WWH couplings [23].

In Figure 7, one can find two representative diagrams out of the complete set for $b\bar{q} \rightarrow H\gamma t\bar{q}$. The W exchange in the t -channel gives rise to a radiative pattern similar to the one in WW fusion, where photon radiation from different quark legs does not interfere destructively. On the other hand, the photon radiation somehow weakens the original cancellation among the different components of the $b\bar{q} \rightarrow tH\bar{q}$ amplitude [22].

As a consequence, the requirement of an extra $p_T > 30 \text{ GeV}$ photon in the $b\bar{q} \rightarrow tH\bar{q}$ channel makes the cross section drop only by an amount $\mathcal{O}(10^{-2})$. In particular, the `AlpGen` estimate for the LO $b\bar{q} \rightarrow tH\bar{q}$ cross section is

$$\sigma(bq \rightarrow H\gamma tq)^{\sqrt{S}=14 \text{ TeV}} = 0.537^{+0.030}_{-0.016} \text{ fb}, \quad (2.21)$$

$$\sigma(bq \rightarrow H\gamma tq)^{\sqrt{S}=33 \text{ TeV}} = 4.19^{+0.42}_{-0.28} \text{ fb}, \quad (2.22)$$

$$\sigma(bq \rightarrow H\gamma tq)^{\sqrt{S}=100 \text{ TeV}} = 29.8^{+4.5}_{-3.8} \text{ fb}, \quad (2.23)$$

where $bq \rightarrow H\gamma tq$ stands for a sum over the two charge-conjugated channels.

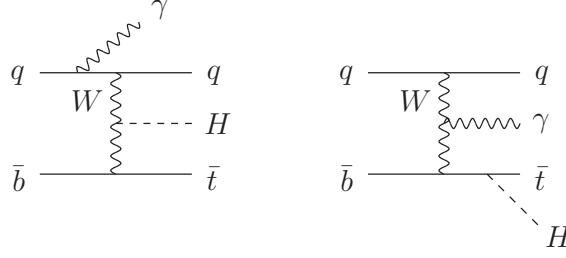


Figure 7. Two representative diagrams for $\bar{b}q \rightarrow H\gamma\bar{t}q$.



Figure 8. Feynman diagrams for $b\bar{b}, c\bar{c} \rightarrow H\gamma$.

2.5 Heavy-quark $b\bar{b}, c\bar{c}$ fusion

Heavy-flavor quark annihilation, where initial $b\bar{b}$ or $c\bar{c}$ pairs come from the sea parton distributions, is the lowest-order channel producing a Higgs boson at hadron colliders. Despite the b - and c -quark Yukawa-coupling suppression, after requiring an extra photon in the $b\bar{b}, c\bar{c} \rightarrow H$ channels (Figure 8), one still gets interesting cross sections. The one-order-of-magnitude difference in the $b\bar{b} \rightarrow H$ and $c\bar{c} \rightarrow H$ cross sections at the LHC (where the coupling ratio $[m_b^{\overline{MS}}(m_H)/m_c^{\overline{MS}}(m_H)]^2 \sim 20$ (cf. Eq. (2.2)) is partly compensated by the larger c -parton distribution) is reduced by a factor $(Q_b/Q_c)^2 = 1/4$ in the $b\bar{b}, c\bar{c} \rightarrow H\gamma$ cross sections, as will be shown in Section 3. The $b\bar{b} \rightarrow H\gamma$ cross section has been evaluated in the SM in [9], and in supersymmetric extensions of the SM in [24].

Our `AlpGen` estimate in the five-flavor scheme (5FS), with running b and c masses evaluated at the m_H scale in the Yukawa couplings, gives as a result

$$\sigma(b\bar{b} \rightarrow H\gamma)^{\sqrt{S}=14\text{ TeV}} = 0.162_{+0.040}^{-0.041} \text{ fb}, \quad (2.24)$$

$$\sigma(b\bar{b} \rightarrow H\gamma)^{\sqrt{S}=33\text{ TeV}} = 0.713_{+0.206}^{-0.202} \text{ fb}, \quad (2.25)$$

$$\sigma(b\bar{b} \rightarrow H\gamma)^{\sqrt{S}=100\text{ TeV}} = 3.51_{+1.20}^{-1.10} \text{ fb}, \quad (2.26)$$

and

$$\sigma(c\bar{c} \rightarrow H\gamma)^{\sqrt{S}=14\text{ TeV}} = 0.072_{+0.010}^{-0.011} \text{ fb}, \quad (2.27)$$

$$\sigma(c\bar{c} \rightarrow H\gamma)^{\sqrt{S}=33\text{ TeV}} = 0.287_{+0.052}^{-0.053} \text{ fb}, \quad (2.28)$$

$$\sigma(c\bar{c} \rightarrow H\gamma)^{\sqrt{S}=100\text{ TeV}} = 1.28_{+0.30}^{-0.29} \text{ fb}. \quad (2.29)$$

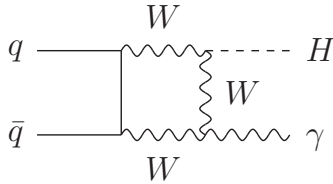


Figure 9. One representative diagram for $\bar{q}q \rightarrow H\gamma$.

$\sigma_{(p_T^{\gamma,j} > 30\text{GeV})}$	$(H)_{14\text{TeV}}$	$(H\gamma)_{14\text{TeV}}$	$(H)_{33\text{TeV}}$	$(H\gamma)_{33\text{TeV}}$	$(H)_{100\text{TeV}}$	$(H\gamma)_{100\text{TeV}}$
$gg, gq, q\bar{q}$	30.8 pb	3.05 fb	137. pb	12.9 fb	745. pb	65.8 fb
VBF	2.37	22.0	8.64	87.3	31.0	325.
WH	1.17	1.88	3.39	5.20	12.1	16.6
ZH	0.625	1.35	1.82	3.49	6.52	10.3
$t\bar{t}H$	0.585	2.55	4.08	17.8	34.3	158.
$tH + \bar{t}H$	0.056	0.536	0.428	4.17	2.18	29.7
$b\bar{b} \rightarrow H$	0.670	0.162	2.82	0.713	14.6	3.51
$c\bar{c} \rightarrow H$	0.069	0.072	0.265	0.287	1.20	1.28

Table 1. Cross sections for $H\gamma$ associated production in pp collisions at 14 TeV, 33 TeV, and 100 TeV, for the dominant channels, for $p_T^{\gamma,j} > 30$ GeV. For comparison, also the cross sections for the corresponding channels without hard-photon radiation are reported, where the first row ($gg, gq, q\bar{q}$) refers to the sum of the Higgs and Higgs-plus-one-jet contributions (see text). All cross sections are at LO, and computed via `AlpGen`. The complete set of selection cuts applied is described in the text.

Note that, although the $gg, q\bar{q} \rightarrow Ht\bar{t}$ and $b\bar{b} \rightarrow H$ cross sections are comparable at 14 TeV (*cf.* Table 1, next Section), the request of an extra photon depletes the $b\bar{b} \rightarrow H$ with respect to not only the $gg, q\bar{q} \rightarrow Ht\bar{t}$ channel, but also the single-top $bq \rightarrow tHq$ process (*cf.* Eqs. (2.18) and (2.21)).

2.6 Electroweak $\bar{q}q \rightarrow H\gamma$ production

A further channel mildly contributing to the $H\gamma$ associated production is $q\bar{q} \rightarrow H\gamma$ that occurs via light-quark annihilation, going through s -channel γ and Z exchange, involving a $\gamma\gamma H$ and $Z\gamma H$ triangle loop of top quarks or W 's, and box diagrams with W 's and light quarks running in the loop. Figure 9 shows one diagram out of the complete set. The corresponding cross sections have been computed at the Tevatron and the LHC [9], and found to be quite smaller than the heavy-flavor tree-level $Q\bar{Q} \rightarrow H\gamma$ contribution to the $H\gamma$ final state at the LHC. We will then neglect the corresponding rates in the present discussion.

3 Comparison of rates and distributions

In the previous section, we detailed the LO cross sections for the dominant $H\gamma$ production channels at different c.m. energies. We included a study of the scale dependence in order

to get a flavor of NLO correction effects. We are now going to discuss how the LO central values (*i.e.*, computed for $\mu = m_H$) for cross sections of different processes compare, in order to pinpoint the main components of the $H\gamma$ inclusive production. We also confront the cross sections of various $H\gamma$ channels with the cross sections of the corresponding Higgs production channels where no high- p_T photon is radiated. This will make manifest the fact that the presence of an extra photon in the final state deeply affects the hierarchy of importance for Higgs production channels.

In Table 1, we show, for $\sqrt{S} = 14$ TeV, 33 TeV, and 100 TeV, LO cross sections computed via `AlpGen`, with the parton distribution set CTEQ5L, and the factorization and renormalization scale at the common value $\mu = m_H$. We assume the setup defined by Eqs. (2.1) and (2.2), implying a cut $p_T^{\gamma,j} > 30$ GeV on the photon and (if present) final-jets transverse momenta. In Table 1, we alternate columns referring to cross sections for main Higgs production channels (with no final photon), named $(H)_{\sqrt{S}}$, with the corresponding ones where an extra photon is required, named $(H\gamma)_{\sqrt{S}}$.

Note that the first process considered (first row, named $gg, qg, \bar{q}q$), corresponding to the original gluon-fusion Higgs production, includes in its *photon-less* $(H)_{\sqrt{S}}$ component not only $gg \rightarrow H$, but also the Higgs+jet channel proceeding at LO via the $gg, qg(\bar{q}g), \bar{q}q \rightarrow Hg, q(\bar{q}), g$ scattering, mediated by an effective ggH vertex. This is to match the corresponding $H\gamma$ top-loop component, which requires at the lowest order an extra final parton in the processes $gg, qg(\bar{q}g), \bar{q}q \rightarrow H\gamma g, q(\bar{q}), g$ (as discussed in Section 2.1)⁶. Note also that, the corresponding $(H\gamma)_{\sqrt{S}}$ component gets only a minor contribution from the pentagon $gg \rightarrow H\gamma g$ process (see again Section 2.1).

By looking at cross sections in Table 1, it gets particularly clear that the requirement of an extra high- p_T photon suppresses the original Higgs production rates by an amount that is widely dependent on the process. Top-loop production turns out to drop by a factor 10^{-4} at all c.m. energies considered, and is the most suppressed process. Slightly less suppressed (by a factor $\sim 2.4 \cdot 10^{-4}$) is the $b\bar{b} \rightarrow H$ rate. On the contrary, both VBF and single-top production loose just a factor 10^{-2} when adding a photon, and present the least decreased rates. The rates for all other channels drop by a few 10^{-3} , with a suppression factor increasing going from $c\bar{c} \rightarrow H$ (10^{-3}), up to WH, ZH ($\sim 1.3 \cdot 10^{-3} - 2 \cdot 10^{-3}$), and $t\bar{t}H$ ($\sim 4 \cdot 10^{-3}$).

At the LHC, the most abundant $H\gamma$ production arises from VBF (22 fb), with one-order-of-magnitude lower contributions from VH (3.2 fb), top-loop production (3.1 fb), and $t\bar{t}H$ (2.6 fb). At larger c.m. energies, VBF is still by far dominant, but the relative weight of top-loop and direct top production increases considerably. At $\sqrt{S} \simeq 100$ TeV, VBF is about 0.31 pb (*i.e.*, more than 50% of the total), $t\bar{t}H$ is about 0.16 pb, and all the remaining $H\gamma$ channels sum up to about 0.12 pb.

In Table 2, we present the corresponding rates at $\sqrt{S} \simeq 8$ and 13 GeV, with same conventions as in Table 1. The $(H\gamma)_{\sqrt{S}}$ cross sections, defined as in Tables 1 and 2, for all

⁶For instance, at 14(100) TeV, the LO $gg, qg, \bar{q}q$ component of $(H)_{14(100)\text{TeV}}$ [that is 30.8(745).pb] is made up of 19.7(415).pb, coming from the $gg \rightarrow H$ LO cross section, plus 7.9(274).pb, arising from the $gg \rightarrow Hg$ LO cross section, plus 3.1(56).pb, from $qg(\bar{q}g) \rightarrow Hq(\bar{q})$, with negligible $q\bar{q} \rightarrow Hg$ contributions.

$\sigma_{(p_T^{\gamma,j} > 30 \text{ GeV})}$	$(H)_{8\text{TeV}}$	$(H\gamma)_{8\text{TeV}}$	$(H)_{13\text{TeV}}$	$(H\gamma)_{13\text{TeV}}$
$gg, gq, q\bar{q}$	10.3 pb	1.03 fb	26.8 pb	2.68 fb
VBF	0.844	6.93	2.08	18.8
WH	0.552	0.858	1.07	1.70
ZH	0.291	0.637	0.567	1.23
$t\bar{t}H$	0.137	0.608	0.487	2.13
$tH + \bar{t}H$	0.012	0.095	0.046	0.431
$b\bar{b} \rightarrow H$	0.232	0.051	0.586	0.140
$c\bar{c} \rightarrow H$	0.026	0.024	0.061	0.062

Table 2. Same as in Table 1 at $\sqrt{S} = 8$ TeV and 13 TeV.

$\sigma_{(p_T^{\gamma,j} > 20 \text{ GeV})}$	$(H)_{14\text{TeV}}$	$(H\gamma)_{14\text{TeV}}$
$gg, gq, q\bar{q}$	35.7 pb	4.61 fb
VBF	3.02	38.8
WH	1.17	2.85
ZH	0.625	2.01
$t\bar{t}H$	0.585	3.32
$tH + \bar{t}H$	0.061	0.842
$b\bar{b} \rightarrow H$	0.670	0.308
$c\bar{c} \rightarrow H$	0.069	0.135

Table 3. Same as in Table 1 at $\sqrt{S} = 14$ TeV, and for $p_T^{\gamma,j} > 20$ GeV.

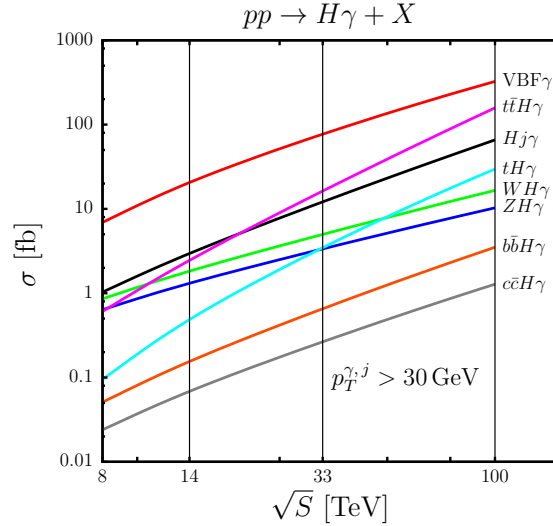


Figure 10. Cross sections for $pp \rightarrow H\gamma + X$ with same kinematical cuts as in Tables 1 and 2.

processes versus \sqrt{S} are also plotted in Figure 10, which clearly shows the new hierarchy of different Higgs production channels.

We stress that all the rates (and corresponding hierarchies) presented in Tables 1 and

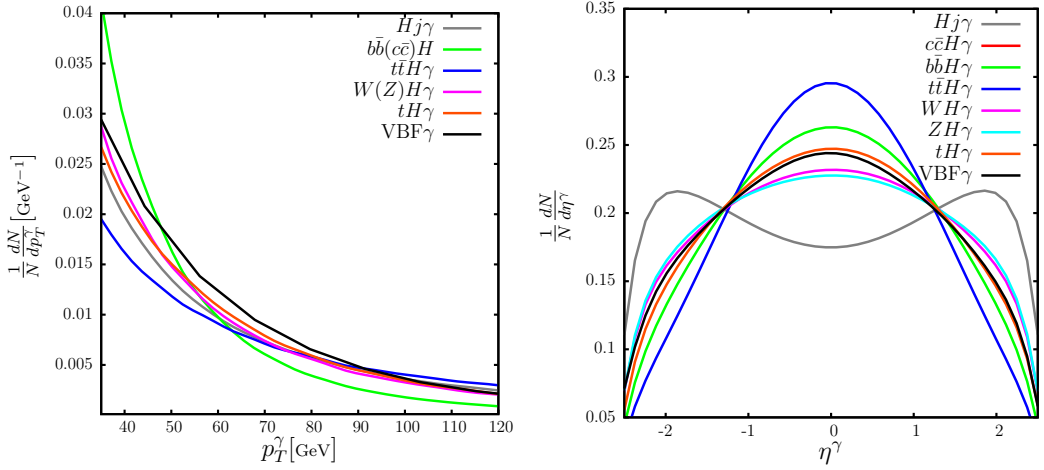


Figure 11. Photon transverse momentum and pseudorapidity distributions at $\sqrt{S} = 14$ TeV. Conventions are detailed in the text.

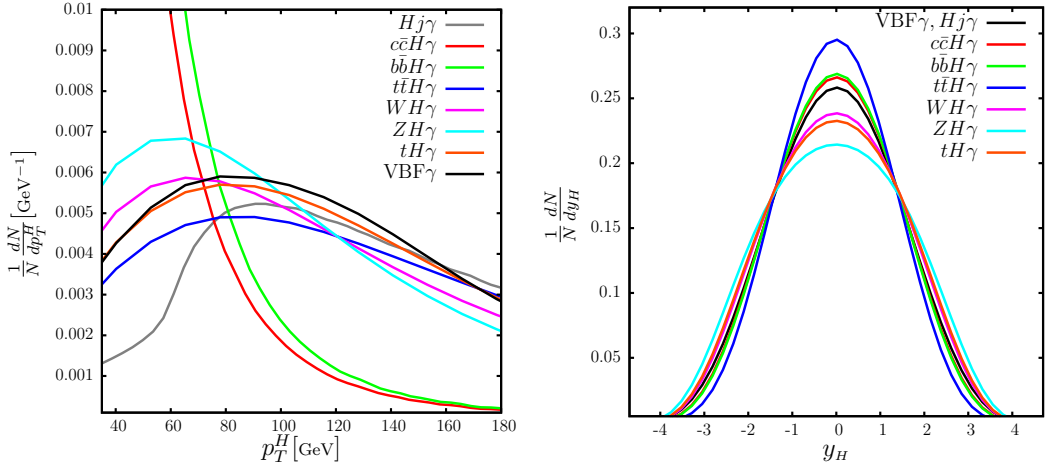


Figure 12. Higgs transverse momentum and rapidity distributions at $\sqrt{S} = 14$ TeV. Conventions are detailed in the text.

2 somewhat depend on the kinematical selection of the final state. On the one hand, all rates are affected by the choice of the photon p_T cut (in general not in a universal way). On the other hand, the channels including jets among the final products are also sensitive to the jet selection. A different selection can hence affect in principle the relative weight of channels.

In Table 3, we present results at 14 TeV, when one relaxes the $p_T^{\gamma,j} > 30$ GeV cuts in Eq. (2.1) down to the less strict selection $p_T^{\gamma,j} > 20$ GeV, the latter being also quite realistic at the LHC energies. The most affected channels are VBF and the heavy-quark fusion channels. The former is quite dependent on both p_T^γ and p_T^j cuts, and as a consequence doubles its rate, the latter are, among the processes considered, the most sensitive to the p_T^γ cut.

Indeed, the impact of a change in the kinematical selection can be guessed by looking at the various kinematical distributions for the different $H\gamma$ channels, which are shown

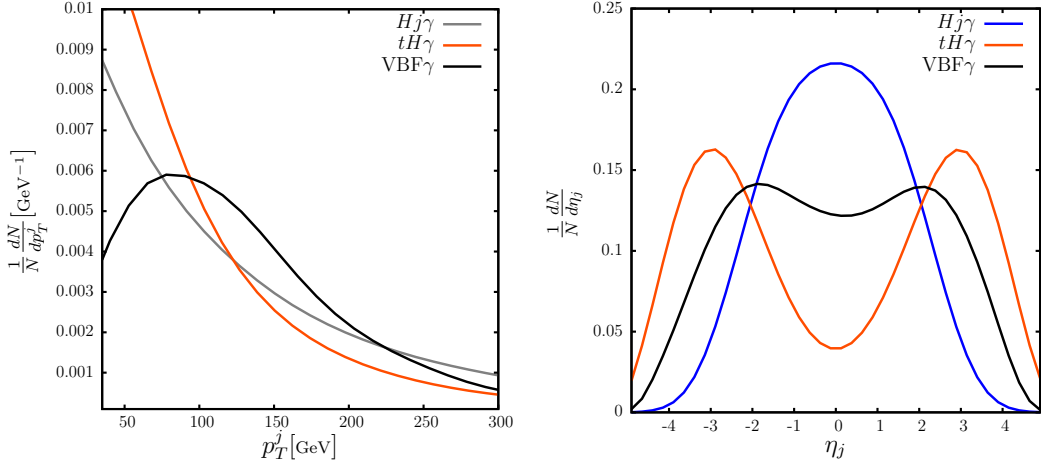


Figure 13. Jet transverse momentum and rapidity distributions at $\sqrt{S} = 14$ TeV. Conventions are detailed in the text.

in Figures 11, 12, and 13, for $\sqrt{S} = 14$ TeV. All distributions are normalized to unity, after applying the kinematical cuts in Eq. (2.1). Distributions detailed by the lines named “ $Hj\gamma$ ” refer to the $gg, q\bar{q}, q\bar{q}$ channels mediated by the effective ggH vertex. One can see that the rate dependence on the photon, Higgs, and jet momenta of various processes can partly alter their relative weight when changing the kinematical selection. In Figure 11, the heavy-quark fusion $b\bar{b}, c\bar{c} \rightarrow H\gamma$ channels present the steepest dependence on p_T^γ , while $H\gamma t\bar{t}$ shows the mildest dependence among the channels considered. The p_T^H dependence in Figure 12 is somewhat more structured. All the processes but $b\bar{b}, c\bar{c} \rightarrow H\gamma$ show the maximum of p_T^H distributions at a quite large p_T^H value. The VBF γ channel (where by VBF γ we name the $H\gamma$ production via VBF) shows the typical $p_T^H \sim M_W$ maximum, which is also present in the basic VBF Higgs production. On the other hand, the $Hj\gamma$ channel, mostly arising from $qg \rightarrow H\gamma q$, has an even higher average p_T^H , since in this case the photon tends to be collinear with the initial/final quark, and the Higgs boson p_T has to balance the p_T of the $j\gamma$ system, each component of which is required to have $p_T > 30$ GeV. In Figure 13, we detail the jet distributions for the few processes where at least one jet is present in the final state.

4 Conclusions

We have made a general analysis of the processes giving rise to final states containing a Higgs boson and a high- p_T photon in proton collisions at different c.m. energies, relevant at the LHC and future colliders. We showed that the request of an extra photon in Higgs production widely affects the normal hierarchy in the main Higgs production processes. In particular, most of the $H\gamma$ signal derives in general from the VBF production.

At the LHC, for $p_T^{\gamma,j} > 20$ GeV, VBF accounts for more than 70% of the $H\gamma$ final states in a LO analysis. The second most important process is the one mediated by the top-loop effective ggH coupling which is responsible for about 9% of the production, although contributing only slightly more than the $t\bar{t}H$ direct top production, and a bit less than the total WH/ZH associated production. At larger c.m. energies (in particular at $\sqrt{S} \gtrsim 33$

TeV), $t\bar{t}H$ gets the upper hand, and becomes the second (following VBF) most relevant process.

As a result, asking for an extra photon in Higgs production reverses the order of importance of the gluon-fusion and VBF mechanisms. Remarkably, the emission of the photon highly suppresses the ZZ fusion component with respect to the WW one in the VBF channel [5]. Hence, the requirement of an extra photon in inclusive Higgs production naturally selects samples with good purity of the WW VBF component, with a rate suppression factor of the order 10^{-2} with respect to the main VBF Higgs channel.

In the present study, we have redone the computation of the $gg \rightarrow H\gamma g$ pentagon amplitude, confirming results recently appeared in the literature. On the other hand, we corrected the relative weight previously assigned to this channel in the production of $H\gamma j$ final states, pointing out the dominant role of processes mediated by the ggH effective coupling. We also computed for the first time the associated Higgs and photon production in processes involving direct production of top pairs and single top.

Of course, the present analysis would be made more robust by a general NLO treatment of all processes. We anyway expect this refinement to keep the general features of the present discussion unchanged.

Accurate predictions for the associated production of a Higgs boson and a photon at the LHC will be crucial not only to test $H\gamma$ interactions, but also in probing new physics effects in the associated production of new scalar particles and photons [25], as well as in searching for resonant three-photon final states [26], [27]. For instance, in case of the production of a scalar ϕ with features departing from the Higgs-boson ones, the present cross-section hierarchy could be widely affected. Non-vanishing terms like $gg\phi\gamma$ in the effective-Lagrangian interactions (violating C parity in the SM case) might resurrect the role of the gluon fusion process as a dominant production channel for the scalar-photon final state, and change the overall picture.

Acknowledgments

This research was supported in part by the European Commission through contracts ERC-2011-AdG No 291377 (LHCtheory) and PITN-GA-2012-316704 (HIGGSTOOLS) and by the Italian Ministry of University and Research under the PRIN project 2010YJ2NYW. R.P. also thanks the project FPA2013-47836-C3-1-P. E.G, F.P., and R.P. acknowledge the CERN TH-Unit for its hospitality and partial support during the preparation of this work. The authors thank the Galileo Galilei Institute for Theoretical Physics for hospitality and INFN for partial support while part of this work was carried out. F.P. would like to thank the Mainz Institute for Theoretical Physics (MITP) for hospitality and support while part of this work was carried out.

A Asymptotic behavior of the top pentagon amplitude for $gg \rightarrow H\gamma g$.

The $g(p_1)g(p_2)g(p_3)\gamma(p_4) \rightarrow H$ amplitude that is relevant for the process in Figure 1 is proportional to

$$A^{\mu_1\mu_2\mu_3\mu_4}(p_1, p_2, p_3, p_4) = \frac{m_t}{i\pi^2} \sum_{\sigma \in S_4(\{1,2,3,4\})} \int d^4q \operatorname{Tr} \left\{ \frac{1}{\not{q}_{\sigma(4)} - m_t} \gamma^{\mu_{\sigma(3)}} \right. \\ \left. \times \frac{1}{\not{q}_{\sigma(3)} - m_t} \gamma^{\mu_{\sigma(2)}} \frac{1}{\not{q}_{\sigma(2)} - m_t} \gamma^{\mu_{\sigma(1)}} \frac{1}{\not{q}_{\sigma(1)} - m_t} \gamma^{\mu_{\sigma(4)}} \frac{1}{\not{q} - m_t} \right\}, \quad (\text{A.1})$$

with

$$q_{\sigma(j)} = q + p_{\sigma(4)} + \sum_{i=1}^{j-1} p_{\sigma(i)}. \quad (\text{A.2})$$

For $m_t \gg m_H, \sqrt{s}$, the pentagon amplitude is well approximated by the following simple expression

$$A_{m_t \rightarrow \infty}^{\mu_1\mu_2\mu_3\mu_4}(p_1, p_2, p_3, p_4) \sim -\frac{1}{m_t^4} \sum_{\substack{j=2 \\ 1 < k \neq j \\ k < l}}^4 \left\{ \frac{32}{9} T_2^{\mu_1\mu_j}(p_1, p_j) T_2^{\mu_k\mu_l}(p_k, p_l) \right. \\ \left. - \frac{112}{45} T_4^{\mu_1\mu_j\mu_k\mu_l}(p_1, p_j, p_k, p_l) \right\}, \quad (\text{A.3})$$

with

$$T_2^{\mu_i\mu_j}(p_i, p_j) = g^{\mu_i\mu_j}(p_i \cdot p_j) - p_i^{\mu_j} p_j^{\mu_i} \quad (\text{A.4})$$

and

$$T_4^{\mu_1\mu_j\mu_k\mu_l}(p_1, p_j, p_k, p_l) = p_1^{\mu_k} p_j^{\mu_l} p_k^{\mu_j} p_l^{\mu_1} + p_1^{\mu_l} p_j^{\mu_k} p_k^{\mu_1} p_l^{\mu_j} \\ + g^{\mu_1\mu_j} g^{\mu_k\mu_l} [(p_1 \cdot p_k)(p_j \cdot p_l) + (p_1 \cdot p_l)(p_j \cdot p_k)] \\ + g^{\mu_1\mu_j} \{ (p_1^{\mu_k} p_j^{\mu_l} + p_1^{\mu_l} p_j^{\mu_k})(p_k \cdot p_l) - p_k^{\mu_l} [p_1^{\mu_k}(p_j \cdot p_l) + p_j^{\mu_k}(p_1 \cdot p_l)] \\ - p_l^{\mu_k} [p_1^{\mu_l}(p_j \cdot p_k) + p_j^{\mu_l}(p_1 \cdot p_k)] \} \\ + g^{\mu_k\mu_l} \{ (p_k^{\mu_1} p_l^{\mu_j} + p_k^{\mu_j} p_l^{\mu_1})(p_1 \cdot p_j) - p_l^{\mu_j} [p_k^{\mu_1}(p_j \cdot p_l) + p_l^{\mu_1}(p_j \cdot p_k)] \\ - p_j^{\mu_1} [p_k^{\mu_j}(p_1 \cdot p_l) + p_l^{\mu_j}(p_1 \cdot p_k)] \}. \quad (\text{A.5})$$

References

- [1] G. Aad *et al.* [ATLAS Collaboration], Phys. Lett. B **716**, 1 (2012) [arXiv:1207.7214 [hep-ex]]; S. Chatrchyan *et al.* [CMS Collaboration], Phys. Lett. B **716**, 30 (2012) [arXiv:1207.7235 [hep-ex]].
- [2] F. Englert and R. Brout, Phys. Rev. Lett. **13**, 321 (1964); P. W. Higgs, Phys. Lett. **12**, 132 (1964); P. W. Higgs, Phys. Rev. Lett. **13**, 508 (1964); G. S. Guralnik, C. R. Hagen and T. W. B. Kibble, Phys. Rev. Lett. **13**, 585 (1964).

- [3] LHC Higgs Cross Section Working Group, *Handbook of LHC Higgs Cross Sections: 1. Inclusive Observables*, CERN-2011-002 (CERN, Geneva, 2011), [arXiv:1101.0593 [hep-ph]]; *2. Differential Distributions*, CERN-2012-002 (CERN, Geneva, 2012), [arXiv:1201.3084 [hep-ph]], S. Dittmaier, C. Mariotti, G. Passarino, and R. Tanaka (Eds.), *3. Higgs Properties*, CERN-2013-004 (CERN, Geneva, 2013), [arXiv:1307.1347 [hep-ph]], S. Heinemeyer, C. Mariotti, G. Passarino, and R. Tanaka (Eds.).
- [4] P. Agrawal and A. Shivaji, *Phys. Lett. B* **741** (2015) 111 [arXiv:1409.8059 [hep-ph]].
- [5] E. Gabrielli, F. Maltoni, B. Mele, M. Moretti, F. Piccinini and R. Pittau, *Nucl. Phys. B* **781** (2007) 64 [hep-ph/0702119 [HEP-PH]].
- [6] K. Arnold, T. Figy, B. Jager and D. Zeppenfeld, *JHEP* **1008** (2010) 088 [arXiv:1006.4237 [hep-ph]].
- [7] S. Mao, W. Neng, L. Gang, M. Wen-Gan, Z. Ren-You, G. Lei, Z. Ya-Jin and G. Jian-You, *Phys. Rev. D* **88:076002** (2013) [arXiv:1310.0946 [hep-ph]].
- [8] X. Shou-Jian, M. Wen-Gan, G. Lei, Z. Ren-You, C. Chong and S. Mao, *J. Phys. G* **42** (2015) 6, 065006 [arXiv:1505.03226 [hep-ph]].
- [9] A. Abbasabadi, D. Bowser-Chao, D. A. Dicus and W. W. Repko, *Phys. Rev. D* **58** (1998) 057301 [hep-ph/9706335].
- [10] M. L. Mangano, M. Moretti, F. Piccinini, R. Pittau and A. D. Polosa, *JHEP* **0307** (2003) 001 [hep-ph/0206293].
- [11] H. L. Lai *et al.* [CTEQ Collaboration], *Eur. Phys. J. C* **12** (2000) 375 doi:10.1007/s100529900196 [hep-ph/9903282].
- [12] $\tilde{\text{A}}\tilde{\text{S}}$ Future Circular Collider Study Kickoff Meeting, Geneva, 12-15 February 2014 $\tilde{\text{A}}\tilde{\text{S}}$. <https://indico.cern.ch/event/282344/>.
- [13] N. Arkani-Hamed, T. Han, M. Mangano and L. T. Wang, arXiv:1511.06495 [hep-ph].
- [14] J. Baglio, A. Djouadi and J. Quevillon, arXiv:1511.07853 [hep-ph].
- [15] A. Andreazza *et al.*, *Frascati Phys. Ser.* **60** (2015) 1.
- [16] G. Ossola, C. G. Papadopoulos and R. Pittau, *Nucl. Phys. B* **763** (2007) 147 [hep-ph/0609007].
- [17] G. Ossola, C. G. Papadopoulos and R. Pittau, *JHEP* **0803** (2008) 042 [arXiv:0711.3596 [hep-ph]].
- [18] A. van Hameren, *Comput. Phys. Commun.* **182** (2011) 2427 [arXiv:1007.4716 [hep-ph]].
- [19] G. Ossola, C. G. Papadopoulos and R. Pittau, *JHEP* **0805** (2008) 004 [arXiv:0802.1876 [hep-ph]].
- [20] R. Kleiss and W. J. Stirling, *Nucl. Phys. B* **262** (1985) 235.
- [21] P. Torrielli, arXiv:1407.1623 [hep-ph].
- [22] T. M. P. Tait and C.-P. Yuan, *Phys. Rev. D* **63** (2000) 014018 [hep-ph/0007298]; F. Maltoni, K. Paul, T. Stelzer and S. Willenbrock, *Phys. Rev. D* **64** (2001) 094023 [hep-ph/0106293]; V. Barger, M. McCaskey and G. Shaughnessy, *Phys. Rev. D* **81** (2010) 034020 [arXiv:0911.1556 [hep-ph]].
- [23] S. Biswas, E. Gabrielli and B. Mele, *JHEP* **1301** (2013) 088 [arXiv:1211.0499 [hep-ph]]; M. Farina, C. Grojean, F. Maltoni, E. Salvioni and A. Thamm, *JHEP* **1305** (2013) 022

[arXiv:1211.3736 [hep-ph]]; S. Biswas, E. Gabrielli, F. Margaroli and B. Mele, JHEP **1307** (2013) 073 [arXiv:1304.1822 [hep-ph]].

[24] E. Gabrielli, B. Mele and J. Rathsman, Phys. Rev. D **77** (2008) 015007 doi:10.1103/PhysRevD.77.015007 [arXiv:0707.0797 [hep-ph]].

[25] X. X. Li, C. X. Yue, J. X. Chen and J. N. Dai, Chin. Phys. C **36** (2012) 485.

[26] N. Toro and I. Yavin, Phys. Rev. D **86** (2012) 055005 doi:10.1103/PhysRevD.86.055005 [arXiv:1202.6377 [hep-ph]].

[27] G. Aad *et al.* [ATLAS Collaboration], arXiv:1509.05051 [hep-ex].